J Shanghai Univ (Engl Ed), 2011, 15(3): 166–172
Digital Object Identifier(DOI): 10.1007/s11741-011-0715-1

Resonant behaviors of ultra-sonic gas atomization nozzle with zero mass-flux jet actuator

ZU Hong-biao (祖洪彪), WANG Zhi-liang (王志亮)
Shanghai Institute of Applied Mathematics and Mechanics, Shanghai Key Laboratory of Mechanics in Energy Engineering, Shanghai University, Shanghai 200072, P. R. China

©Shanghai University and Springer-Verlag Berlin Heidelberg 2011

Abstract The resonant behaviors of an ultra-sonic gas atomization nozzle with a zero mass-flux jet actuator were numerically investigated with FLUENT software by using a double precision unsteady two-dimensional pressure-based solver. The Spalart-Allmaras turbulence model was adopted in the simulations. Numerical results indicated that the oscillation properties of the gas efflux were effectively improved. Several resonatory frequencies corresponding to different vibration modes of gas were distinguished in the nozzle. With the changing of nozzle geometric parameters, different characters among those modes were elucidated by analyzing the propagations of pressure waves.

Keywords spray atomization, ultra-sonic gas atomization nozzle, resonance, numerical simulation
2000 Mathematics Subject Classification 74D05

Introduction

Hartmann[1] found resonance phenomena of a tube while doing experiments in 1919. A lot of research carried out theoretical and experimental works to explain the mechanism of resonance in sonic tubes[2−4]. Grant[5] invented an ultra-sonic gas atomization (USGA) nozzle in spray atomization by using the effects of a Hartmann resonance tube.

Spray atomization is a process of making liquid droplets. In spray forming technology, high-speed gas flow to fragmentize the molten metal jet into small fractals. The nozzle is an important part of a spray atomizer. There are two kinds of atomizing nozzle in use generally, USGA nozzle and high-pressure gas atomization (HPGA) nozzle[6].

The sizes and its distribution of atomized metal droplets can affect the quality of products directly in spray forming technology. Experiments indicate that the small average size and its relative narrow-band distribution of droplets, which is helpful to improve the quality of spray injection products[5,7], and can be produced when introducing oscillations into the gas atomization. Hence, the USGA nozzle is adopted as an apparatus to generate such high frequency oscillating gas efflux owing to its Hartmann resonance effect[8].

Veistinen, *et al.*[9] proposed a "self-adjusting throat" hypothesis to explain how the flow of gas in the nozzle translates from a subsonic jet into a supersonic jet. Assuming a flow of steady, Mansour, *et al.*[10] simulated the flow in USGA nozzle numerically with the flow structure inside the nozzle and downstream outside the nozzle considered. Li, *et al.*[8] investigated the USGA nozzle numerically by the finite volume method based on the Roe solver. They studied the effects of variation of parameters on the oscillation and discussed the mechanism of transition from subsonic to supersonic jet flows.

In this paper, the resonant behaviors of a USGA nozzle with a zero mass-flux jet actuator are numerically investigated with FLUENT software by using a two-dimensional unsteady pressure-based solver with Spalart-Allmaras turbulence model.

1 Mathematical model and algorithm

We created the simplified USGA nozzle model including inflow and outflow ducts and the resonance region. Schematic of computational region and meshes is shown in Fig.1. Resonance tube length and secondary resonance tube length are represented by L_1 and L_2. Lengths of inflow and outflow ducts are represented by L_3 and L_4. The diameter of the tube is d=3.6 mm. The actuator is placed at the right end of the tube.

Received May 20, 2010; Revised Jun.8, 2010
Project supported by the National Natural Science Foundation of China (Grant Nos.10772107, 10702038), the Shanghai Municipal Key Projects on Basic Research (Grant No.08JC1409800), the Innovation Project of Shanghai Municipal Education Commission (Grant No.08YZ10), and the Shanghai Municipal Science and Technology Commission (Grant No.09DZ1141502)
Corresponding author WANG Zhi-liang, Ph D, Assoc Prof, E-mail: wng_zh@shu.edu.cn

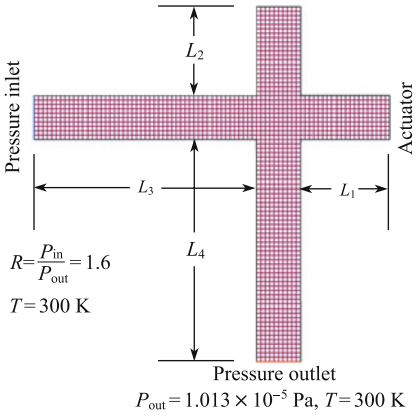

Fig.1 Schematic of computational region and meshes

Computational work was implemented by using FLUENT software, and square grids were generated with GAMBIT software. A double precision unsteady two-dimensional pressure-based solver was chosen. Second order implicit scheme was adopted in time and first order upwind scheme was adopted in space. The Spalart-Allmaras turbulence model was used in the numerical computations. The algorithm of semi-implicit method for pressure-linked equations (SIMPLE) was used to deal with the pressure-velocity coupling.

The Reynolds-averaged Navier-Stokes (RANS) equations were numerically solved which were given as below:

$$\frac{\partial\rho}{\partial t}+\frac{\partial}{\partial x_i}(\rho u_i)=0, \tag{1}$$

$$\frac{\partial}{\partial t}(\rho u_i)+\frac{\partial}{\partial x_i}(\rho u_i u_j)=-\frac{\partial p}{\partial x_i}+\frac{\partial}{\partial x_i}\Big(\mu\Big(\frac{\partial u_i}{\partial x_j}+\frac{\partial u_j}{\partial x_i}-\frac{2}{3}\delta_{ij}\frac{\partial u_i}{\partial x_j}\Big)\Big)+\frac{\partial}{\partial x_j}\Big(-\rho\overline{u_i'u_j'}\Big). \tag{2}$$

In which

$$-\rho\overline{u_i'u_j'}=\mu_t\left(\frac{\partial u_i}{\partial x_j}+\frac{\partial u_j}{\partial x_i}\right), \tag{3}$$

where u_i and u_j represent the x- and y- components of velocity, ρ the density, p the pressure, μ and μ_t the molecular and turbulent viscosity. The turbulent viscosity μ_t was conducted by the Spalart-Allmaras turbulence model.

In Spalart-Allmaras turbulence model, the transported variable $\tilde{\upsilon}$ is identical to the turbulent kinematic viscosity except in the near-wall region. The transport equation for $\tilde{\upsilon}$ is

$$\frac{\partial}{\partial t}(\rho\tilde{\upsilon})+\frac{\partial}{\partial x_i}(\rho\tilde{\upsilon}u_i)=G_v+\frac{1}{\sigma_{\tilde{\upsilon}}}\Big(\frac{\partial}{\partial x_i}\Big((\mu+\rho\tilde{\upsilon})\frac{\partial\tilde{\upsilon}}{\partial x_j}\Big)+C_{b2}\rho\Big(\frac{\partial\tilde{\upsilon}}{\partial x_j}\Big)^2\Big)-Y_v, \tag{4}$$

where G_v is the production of turbulent viscosity, Y_v the destruction of turbulent viscosity, $\sigma_{\tilde{\upsilon}}$ and C_{b2} the constants.

The turbulent viscosity μ_t is computed from $\mu_t=\rho\tilde{\upsilon}f_{v1}$, where the viscous damping function f_{v1} is given by $f_{v1}=\frac{\chi^3}{\chi^3+C_{\upsilon1}^3}$ and $\chi=\frac{\tilde{\upsilon}}{\upsilon}$, where υ is the molecular kinematic viscosity.

The production term is modeled as $G_v=C_{b1}\rho\widetilde{S}\tilde{\upsilon}$, $\widetilde{S}\equiv S+\frac{f_{v2}\tilde{\upsilon}}{\kappa^2d^2}$, $f_{v2}=1-\frac{\chi}{1+\chi f_{v1}}$, and $S\equiv\sqrt{2\Omega_{ij}\Omega_{ij}}$ is a scalar measure of the deformation tensor, $\Omega_{ij}=\frac{\frac{\partial u_i}{\partial x_j}-\frac{\partial u_j}{\partial x_i}}{2}$ the mean rate-of-rotation tensor, C_{b1} and κ the constants, d the distance from the wall.

The destruction term is modeled as $Y_v=C_{w1}\rho f_w(\frac{\tilde{\upsilon}}{d})^2$, $f_w=\sqrt[6]{\frac{(1+C_{w3}^6)}{(g^6+C_{w3}^6)}}g$, $g=r+C_{w2}(r^6-r)$, $r\equiv\frac{\tilde{\upsilon}}{\widetilde{S}\kappa^2d^2}$, C_{w1}, C_{w2} and C_{w3} are constants.

The constants referred above: $\kappa=0.418\,7$, $C_{b1}=0.135\,5$, $C_{b2}=0.622$, $\sigma_{\tilde{\upsilon}}=\frac{2}{3}$, $C_{\upsilon1}=7.1$, $C_{w1}=\frac{C_{b1}}{\kappa^2}+\frac{1+C_{b2}}{\sigma_{\tilde{\upsilon}}}$, $C_{w2}=0.3$ and $C_{w3}=2$.

The pressure of outlet was set to be P_{out}=1.013×10^{-5} Pa, and at the inlet the pressure was chosen to be P_{in}=1.621×10^5 Pa, slightly below which the transonic phenomena will not be clearly observed. The role of the actuator was to generate controllable oscillation, which was represented by a zero mass-flux jet. A no-slip adiabatic wall boundary condition was set at the tube wall. A time-dependent mass flux inlet condition was used as the zero mass-flux jet referred above using user-defined-function (UDF) module in FLUENT as follows:

$$\Phi_{mass}=A_a\sin(2\pi f_a t+\phi), \tag{5}$$

where A_a, f_a and ϕ correspond to the amplitude, frequency and phase of mass influx of actuator, respectively.

2 Verification of computational tools

2.1 Grid size and time-step dependence

For cases $L_1=L_2=2d$, $L_3=L_4=5d$, $R=\frac{P_{in}}{P_{out}}$=2 is the jet pressure ratio and d=3.6 mm is tube diameter, without any actuator herein, grid sizes differ from $\frac{d}{30}$, $\frac{d}{40}$, $\frac{d}{50}$ and $\frac{d}{60}$ were examined, corresponding to a total of 13 500, 24 000, 37 500 and 54 000 cells, respectively. Pressure oscillation at the resonance tube end wall and its spectral analysis is shown in Fig.2. It's clear that amplitudes and frequencies of the pressure oscillation were approximate and the relative error was gradually decreased while gird size is smaller. Finally the $\frac{d}{40}$ grid was chosen in the paper.

The oscillation frequency of the USGA nozzle can be estimated by linear acoustic theory, $\omega=\frac{c}{4L_1}$, where c is the local sound speed and L_1 the length of resonance tube[8,11]. For the case of L_1=L_2=2d, d=3.6 mm, the frequency is about 10 kHz. Four different time-steps were examined and the result is shown in Fig.3. The time step Δt=10^{-6} s was finally chosen in this paper.

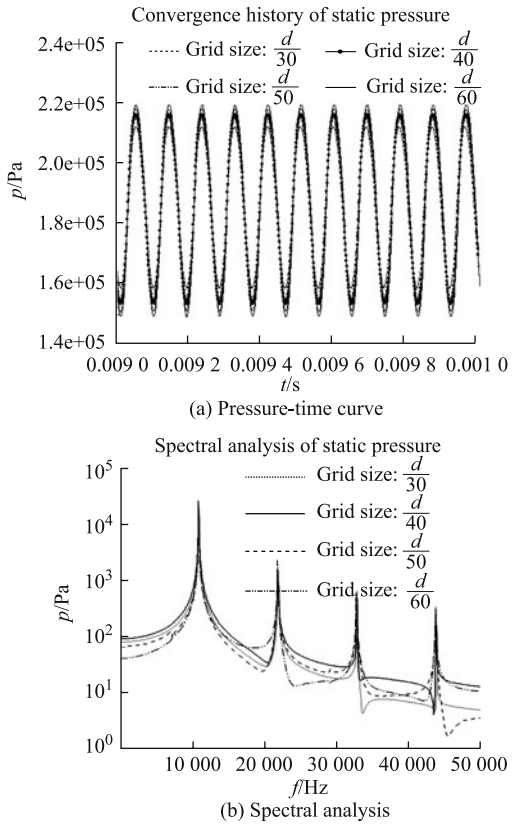

Fig.2 Influences of mesh size

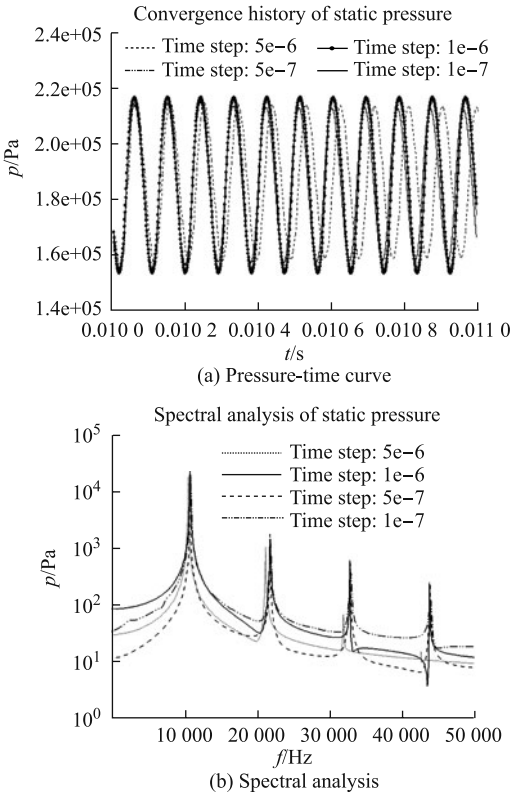

Fig.3 Influences of time-step size

2.2 Comparison with existing results

According to [8], the oscillation frequency f of USGA nozzle equals to Hartmann tube frequency while resonance tube length equals to secondary resonance tube length. We examined cases of $d \leqslant L_1{=}L_2 \leqslant 4d$ and the result given in Fig.4. As distinguished solver and algorithm were used compared with [8], good agreements were derived between the existing results.

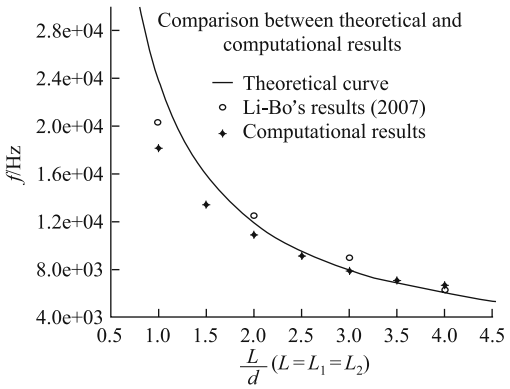

Fig.4 Frequency of the USGA nozzle at the condition of $L_1{=}L_2$

3 Results and discussion

3.1 Resonance behaviors under different frequencies

In order to study on the resonant behaviors of the USGA nozzle with an actuator, we focused on cases $L_1 = L_2 = 2d$, $L_3 = L_4 = 5d$, $R{=}1.6$. Excitation signal at the actuator was given by (5) with $A_a{=}0.1$ kg/s (referring to the inlet mass flow rate is about 1.2 kg/s) and $\varphi{=}0$. The actuator frequency changes in the scope of 0–2ω by every 0.5ω, where ω is oscillation frequency of USGA nozzle without any actuator. For parameters given above, $\omega{=}10\,859$ Hz.

We summarized the amplitudes of mass flow rate A_m and average pressure A_p at the nozzle exit for different actuator frequencies (see Fig.5). Obviously we can find five peaks in each curve, and corresponding horizontal axis of all peaks are given above the curve. Similar tendency is found between the mass flow rate and the average pressure.

From Fig.5 we can also find that the oscillation of the gas efflux is effectively enhanced at certain excitation frequencies. For the case of $f_a{=}1.05\omega$, the amplitude of outflow mass flow rate is 0.189 kg/s, compared with the none-actuator situation (which is 0.058 kg/s), the increment can reach nearly 227%.

3.2 Resonance characteristics

3.2.1 Two different resonance modes

Cases corresponding to the five peaks in Fig.5 are particularly analyzed in this section. Figure 6 shows the

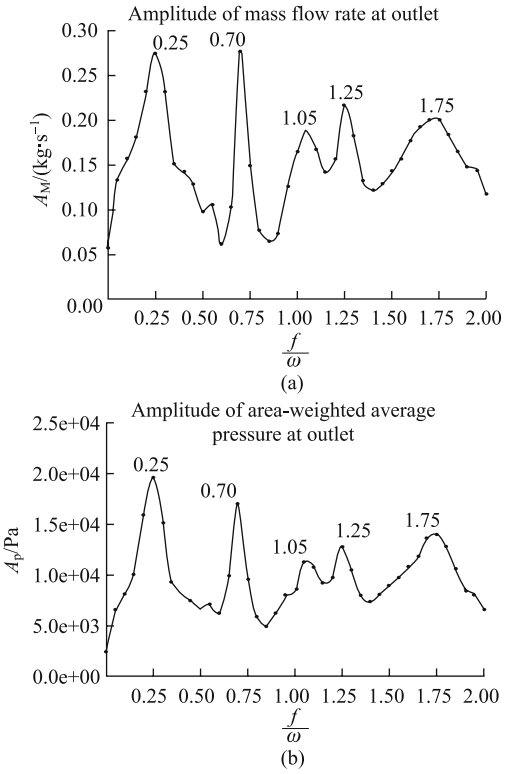

Fig.5 Relationship of amplitude of outflow mass flow rate (a)pressure (b) with frequency

monitor histories of mass flow rate at the nozzle exit and spectral analysis results while f_a=0.25ω, f_a=0.70ω and f_a=1.05ω. For the cases of f_a=1.25ω and f_a=1.75ω, the properties are similar with f_a=0.25ω.

As is shown in Fig.6, for cases f_a=0.70ω and of f_a=1.05ω, the dominant frequency is simplex and the amplitude of outflow mass flow rate oscillation is permanent. In contrast, for the cases of f_a=0.25ω (f_a=1.25ω and f_a=1.75ω similarly), the frequency spectrum is complicated, and the amplitude of gas oscillation varys periodically.

Resonance phenomenon is occurred between the natural frequency of the USGA nozzle and the actuator frequency for the case of f_a=1.05ω, causing a large increase in amplitude. However, the flow structure is different for case f_a=0.70ω. In order to describe the difference, pressure distributions at different times in one period T are shown in Figs.7 and 8.

(i) For the case of f_a=0.70ω as depicted in Fig.7, at time t_0, an expansion wave and a compression wave states at resonance tube mouth and secondary resonance tube mouth respectively, and those pressure waves will propagate towards end of the tube (see Fig.7(a)). After the expansion wave and the compression wave reach at the end of resonance tube and secondary resonance tube end respectively, the waves rebound there and then back-propagate (see Fig.7(b)). Because of the existence of the actuator, the compression wave reaches the "cross" earlier than the expansion wave. Driven by the resonance tube expansion wave, another compression wave which will propagate towards the inflow is generated (see Fig.7(c)). The resonance tube expansion waves then rebound at the "cross" and transform

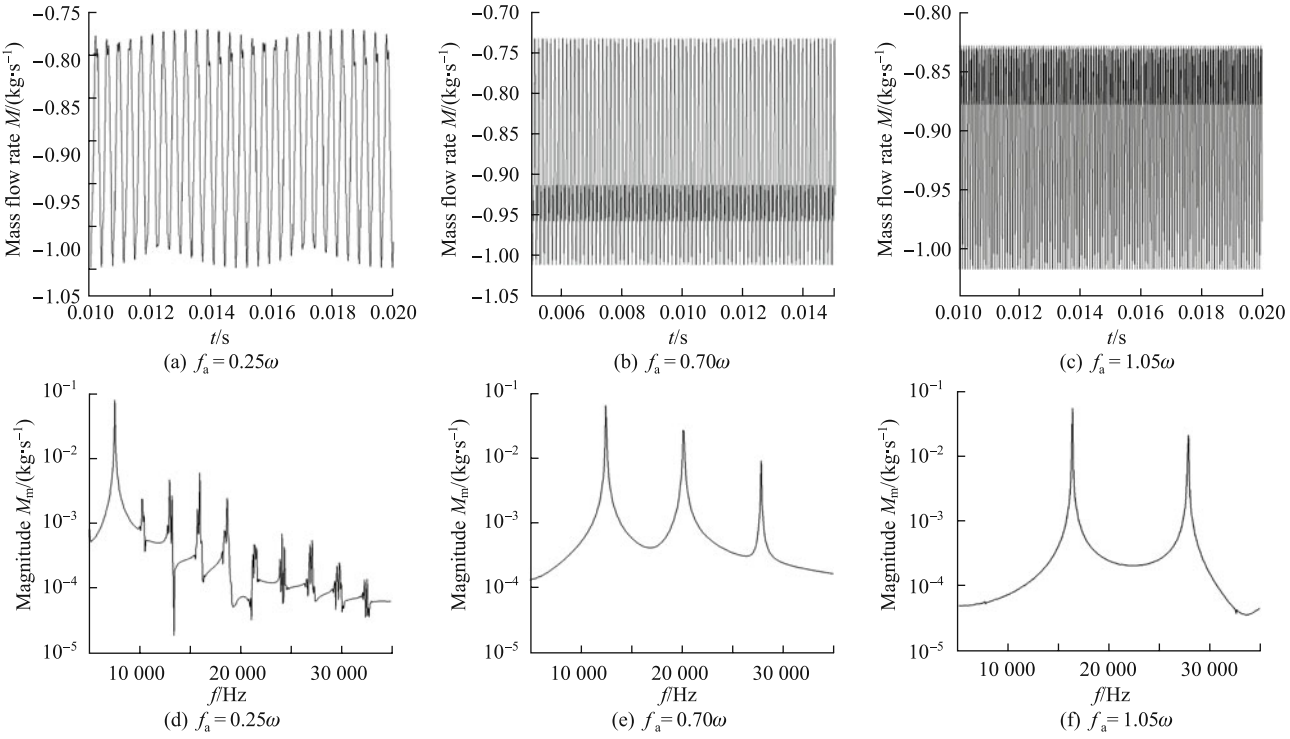

Fig.6 Outflow mass flow rate M and spectral analysis

into another pair of compression wave and expansion wave, propagating towards the resonance tube and the secondary resonance tube respectively (see Fig.7(d)). Then those pressure waves rebound at the tube end and propagate towards the "cross" again. Finally at t_4, pressure distribution of the flow field reach back to time t_0 situation, and a closed cycle is completed (see Fig.7(e)).

(ii) For the case of f_a=1.05ω as shown in Fig.8, the pressure wave propagation process is significantly different from that Fig.7 expresses. The key distinction appears as there is none upstream spread pressure wave in Fig.8. Here f_a=1.05ω, which means the gas oscillation frequencies are approximated in resonance tube and secondary resonance tube. Expansion wave and

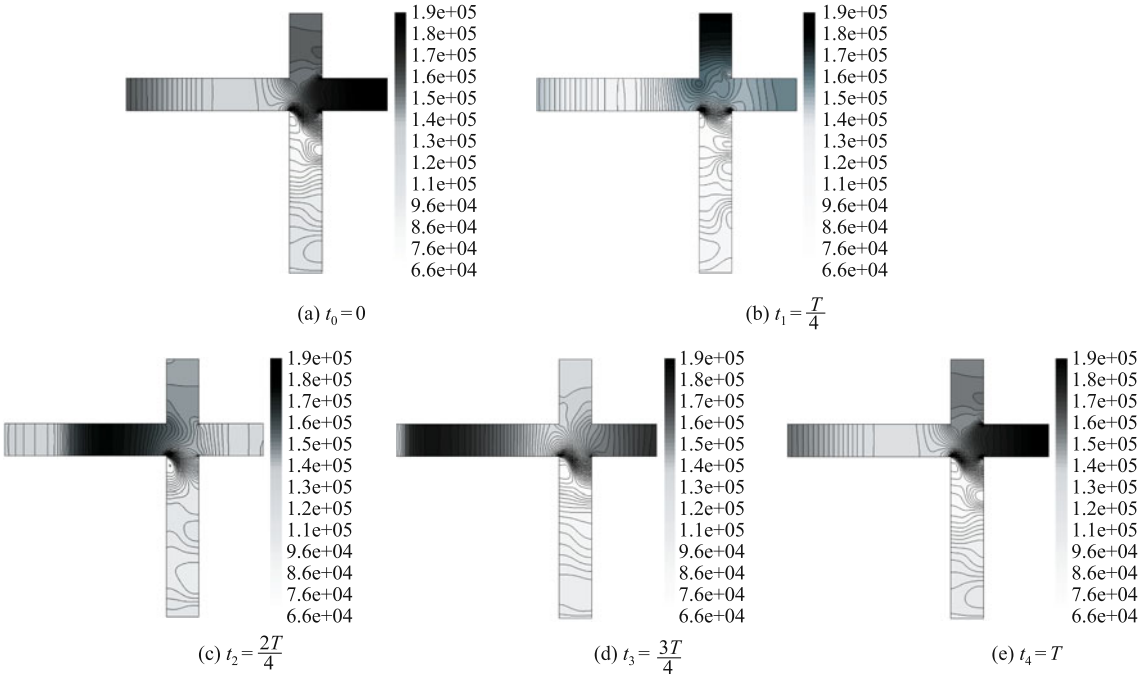

Fig.7 Pressure distribution inside the nozzle in one period at f_a=0.70ω

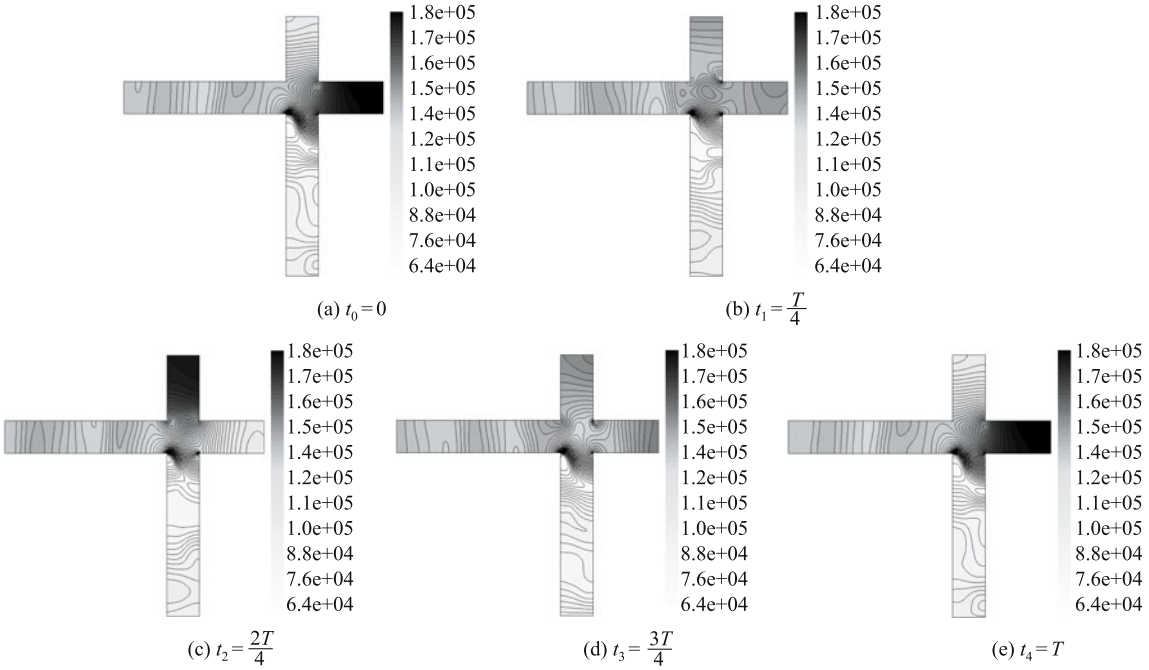

Fig.8 Pressure distribution inside the nozzle in one period at f_a=1.05ω

compression wave propagate alternately in the two resonance tubes, which is homoplastical with USGA nozzle without any actuator as introduced in [8].

We can summary the aforementioned process here: Pressure waves in secondary resonance tube propagated at the local sound speed, while, the propagation speed of the pressure waves in resonance tube is affected by the actuator. If the actuator frequency is far away from intrinsic frequency, some "gas blocking" phenomena will happen in the "cross" location, which lead an upstream spread pressure wave in the inflow duct. In this situation, the inflow duct is involved in the resonance behavior, and we call it "Global mode". On the other hand, however, if actuator frequency is approximate with intrinsic frequency, the oscillation is generally generated by the resonance tube and the secondary resonance tube, and we call it "Hartmann mode".

3.2.2 Two basic frequencies of the nozzle

Consider Figs.5 and 6, f_a=0.7ω is obviously different from the other excitation frequencies. Referring to the "Global mode" discussion, we can figure out that 0.70ω is another basic frequency besides of ω and is determined by L_1, L_2 and L_3. The Hartmann resonance ω corresponds to the linear acoustic quarter-wavelength theory, and the form of quarter-wave-length frequency can be denoted as f_{QWL}. The global-mode frequency is written as f_{GV}.

As is shown in Fig.7, by the pressure wave propagation process we can foresee that f_{GV} will decrease with the increase of L_3 if other conditions are unchanged. In order to verify this, we study two additional cases, L_3=7d and L_3=9d, respectively. The amplitude of outflow mass flow rate is plotted as a continuous curve, as shown in Fig.9 (corresponding to Fig.6). It can be seen that with L_3 increased from 5d to 9d, and f_{GV} decreases from 0.70ω to 0.45ω, while f_{QWL} remains to be unchanged on contrast.

The frequencies of f_a=0.25ω, f_a=1.25ω and f_a= 1.75ω in Fig.5 are the harmonic excitations caused by nonlinear interaction between waves[12].

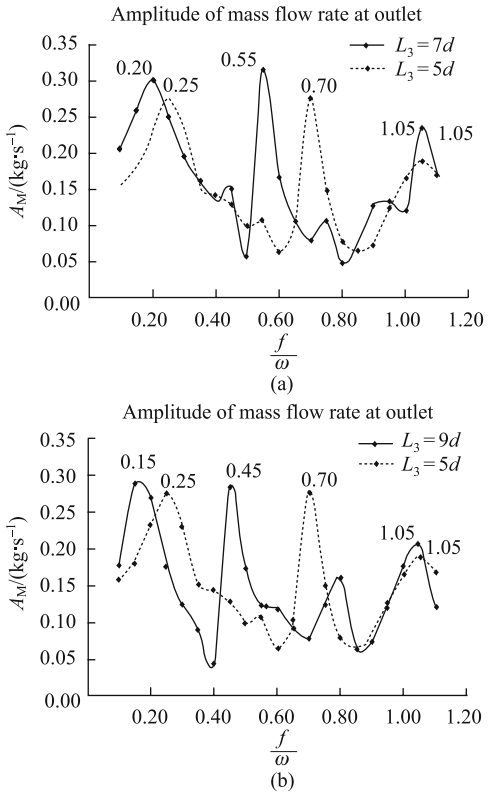

Fig.9 Relationship of amplitude of outflow mass flow rate with frequency at different L_3

4 Conclusions

The resonant behaviors of a USGA nozzle were numerically investigated with the FLUENT software. Verification cases show that the numerical results are comparable with the known simulations and experimental data.

On such a basis, this work, for the first time, proposes of using a zero mass-flux jet actuator to enhance the resonance effects of a USGA nozzle[13]. Numerical results show that the actuator do play big roles, mainly, on the oscillations about two aspects: (i) Multiple resonatory frequencies corresponding to different vibration modes of gas in the nozzle are stimulated; (ii) The amplitudes of oscillations may increase dramatically, which means acoustic wave energy can be effectively amplified.

The simulations also indicate that there are several intrinsic resonatory frequencies existing in the USGA nozzle, not just the well-known quarter-wave-length frequency f_{QWL}. Among those frequencies, two are deduced to be the basic ones. Besides f_{QWL}, which is dominated by the geometry of local resonant tube, a global-mode frequency f_{GV} is identified owing to the whole geometric structure of USGA nozzle, which is a new finding by this work.

Acknowledgment

The study was pushed forward under the guidance of Prof. ZHOU Zhe-wei and Prof. HU Guo-hui and originated from one of Prof. ZHOU's National Science Foundation of China Projects.

References

[1] Hartmann J, Trolle B. A new acoustic generator. The air-jet-generator [J]. Journal of Scientific Instruments, 1927, 4(4): 101–111.

[2] Raman G, Srinivasan K. The powered resonance tube: From Hartmann's discovery to current active flow control applications [J]. Progress in Aerospace Sciences, 2009, 45(4/5): 97–123.

[3] Naraymanan S, Bhave P, Srinivasan K, Ramanurthi K, Sundararajan T. Spectra and directivity of a Hartmann whistle [J]. Journal of Sound and Vibration, 2009, 321(3/5): 875–892.

[4] Narayanan S, Srinivasan K, Ramamurthi K, Sundararajan T. Acoustic characteristics of chamfered Hartmann whistles [J]. Journal of Sound and Vibration, 2011, 330: 2470–2496.

[5] Grant N J. Rapid solidification of metallic particulates [J]. Journal of Metals, 1983, 35(1): 20–27.

[6] Ayres J D, Anderson I E. Method for generating fine sprays of molten metal for spray coating and powder making: United States, No. 4619845 [P]. Oct. 28, 1986.

[7] Rai G, Lavernia E J, Grant N J. Powder size and distribution in ultrasonic gas atomization [J]. Journal of Metals, 1985, 37(8): 22–26.

[8] Li B, Hu G H, Zhou Z W. Numerical simulation of flow in Hartmann resonance tube and flow in ultrasonic gas atomizer [J]. Applied Mathematics and Mechanics (English Edition), 2007, 28(11): 1415–1426.

[9] Veistinen M K, Lavernia E J, Baram J C. Grant N J. Jet behavior in ultrasonic gas atomization [J]. The International Journal of Powder Metallurgy, 1989, 25(2): 89–92.

[10] Mansour A, Chigier N, Shih T I P, Kozarek R L. The effects of the Hartman cavity on the performance of the USGA nozzle needed for aluminum spray forming [J]. Atomization and Sprays, 1998, 8(1): 1–24.

[11] Brocher E, Maresca A, Bournay M H. Fluid dynamics of the resonance tube [J]. Journal of Fluid Mechanics, 1970, 43(2): 369–384.

[12] Drazin P G, Reid W H. Hydrodynamic stability [M]. Cambridge, Eng: Cambridge University Press, 1981: 387–398.

[13] Wang Z L. Actuator driven ultra-sonic gas atomization nozzle: P. R. China, Application No. 200810203978 [P]. May 30, 2011.

(Editor CHEN Hai-qing)